Electronic tuning of integrated blue-violet GaN tunable coupled-cavity laser

O. Guziy,[1,a] S. Grzanka,[2,3] M. Leszczyński,[2,3] P. Perlin,[2,3] M. Schemmann,[4] and H. W. M. Salemink[1]

[1]*Kavli Institute of Nanoscience, Delft University of Technology, Lorentzweg 1, 2628 CJ Delft, The Netherlands*
[2]*Institute of High Pressure Physics, Sokolowska 29/37, 01-142 Warsaw, Poland*
[3]*TopGaN Ltd., Sokolowska 29/37, 01-142 Warsaw, Poland*
[4]*FOCE Technology Intl BV, The Netherlands*

(Received 16 April 2012; accepted 20 July 2012; published online 1 August 2012)

We demonstrate an integrated tunable coupled-cavity InGaN/GaN laser with the emission wavelength centered on 409 nm. The electronic tuning range was 1.6 nm and threshold currents were 650 mA per cavity for 8.7-μm-wide laser ridges. Multimode laser emission with an average full width at half maximum of 0.3 nm was observed. We estimate the refractive index change due to free-carrier injection and optical gain to explain the experimental tuning range. [http://dx.doi.org/10.1063/1.4742971]

I. INTRODUCTION

Tunable blue-violet laser diodes are of increasing interest for a wide range of applications, including optical data storage, chemical or biological hazard detection, laser-induced fluorescence spectroscopy, photobiology and medical diagnostics.[1,2] Currently, nonlinear optical conversion of tunable infrared lasers is widely used to obtain tunable blue lasers. Optical parametric oscillation[3] or sum-frequency mixing of dye lasers[4] and Ti-sapphire lasers[5] are examples of this approach. Although external-cavity tunable semiconductor lasers have been reported for the blue range,[6,7] their main disadvantage for applications is that they require precise mechanics and alignment. The complexity of the approaches mentioned above leads to bulky and expensive systems, whereas low cost and portability are desirable features for most applications.[8] By introducing the integrated coupled-cavity design to GaN semiconductor lasers, one can achieve a practical tuning range and higher reliability while keeping device size, cost and complexity low. GaN-coupled cavity lasers open the way to inexpensive blue-violet tunable lasers because they lend themselves to mass-production fabrication techniques.

Coupled-cavity lasers consist of two Fabry–Perot cavities separated by a sub-wavelength air gap (see Fig. 1). The coupled-cavity concept can be used to tune the laser emission over the wavelength range where substantial gain is available.[9] In this paper we present a multimode index-guided InGaN laser.

II. FABRICATION

Lasers were fabricated from an AlGaN/GaN/InGaN multiple quantum well laser structure emitting at 409 nm and grown on bulk gallium-nitride crystals obtained with the high-nitrogen-pressure solution method. The GaN substrate was grown at very high nitrogen pressure and therefore has a low dislocation density (below 10^5 cm^{-2}).[10] The laser structure (Table I) consists of 360 and

[a]Author to whom correspondence should be addressed. Electronic mail: o.guziy@tudelft.nl

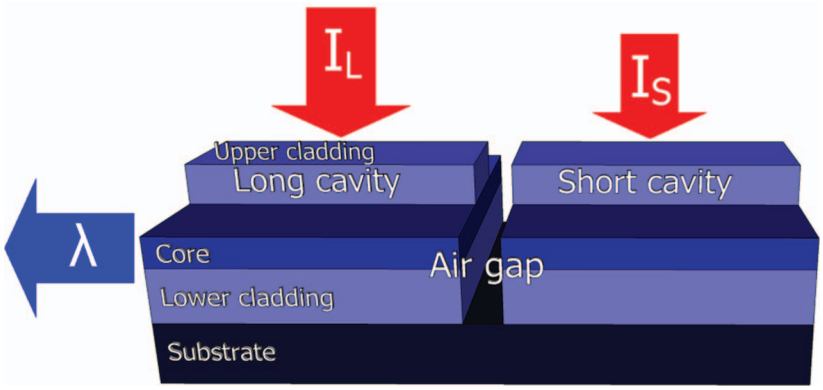

FIG. 1. Fabry–Perot coupled-cavity laser with sub-wavelength air gap can be tuned by varying currents in the short and long cavities.

TABLE I. Laser diode structure details.

Contact layer	30 nm GaN:Mg ($2 \cdot 10^{18}$ cm^{-3})
Top Cladding	330 nm $Al_{0.08}GaN_{0.92}N$: Mg ($2 \cdot 10^{18}$ cm^{-3})
Waveguide-top	80 nm GaN:Mg ($2 \cdot 10^{18}$ cm^{-3})
Blocking layer	20 nm $Al_{0.20}Ga_{0.80}N$:Mg
MQW	3.5 nm InGaN × 3
	10nm $In_{0.02}Ga_{0.98}N$
Waveguide - bottom	40 nm $In_{0.02}Ga_{0.98}N$
	50 nm GaN
Bottom cladding	830 nm $Al_{0.08}GaN_{0.92}N$: Si ($5 \cdot 10^{18}$ cm^{-3})
Substrate	Bulk GaN substrate

830-nm-thick upper and lower AlGaN cladding layers, respectively, and a 230-nm-thick GaN core layer with 3 × 3.5 nm InGaN quantum wells.

The laser ridges are defined by optical lithography and Cl_2/Ar inductively coupled plasma etching. The sidewalls of the ridges were passivated with 200 nm of SiO_2 and an opening was etched into the top of the ridge to provide contact. Thin Ni/Au electron-beam-evaporated contacts were patterned by optical lithography and liftoff. Subsequently, 3-μm-thick gold contacts were electroplated on top of the evaporated contacts, providing both current injection and heat removal from the laser ridge. After thinning the substrate, a Ni/Au contact was evaporated on the *n*-type side of the substrate. The wafer was cleaved into dual-section lasers. A 26-μm-wide gap was left between the two contacts to provide electrical insulation of each section and to facilitate milling of a 340-nm-wide and 1.2-μm-deep slot in the laser ridge by a focused ion beam (FIB). For this purpose a dual-beam system FEI Strata DB 235 with Ga+ ions at 30 kV acceleration voltage and 50 nA beam current was used. Milling of the air slot resulted in long front and short back Fabry–Perot cavities with lengths of 701 and 689 μm, respectively. High-reflection coatings were applied on both front and back cleaved facets. The intensity reflection coefficients are estimated to be $R_{\text{front}} = R_{\text{back}} = 90\%$.

III. EXPERIMENTAL CHARACTERIZATION

GaN lasers were mounted on a copper heat sink onto a thermoelectric cooler with temperature controller. Optical spectra were measured as a function of currents in the short and long cavities. For this purpose a computer-controlled, dual-channel, pulse-driving unit was used to drive the laser. To minimize thermal heating of the device at high currents, 200-ns pulses with a repetition rate of 50 kHz (duty cycle of 1%) were used. Two calibrated coils were placed around the contact wires to monitor the current with minimal distortion to the circuit. Laser emission was collected

from the front facet and collimated by an AR-coated aspheric lens with a focal length of 2.8 mm (Newport 5721-H-A). Spectral measurements were taken by an Ocean Optics HR4000 spectrometer with 0.045-nm resolution. All measurements discussed in this paper were taken with the same laser device.

IV. SIMULATIONS

Semiconductor lasers can be tuned by varying the laser driving current. Changing the refractive index by varying the current shifts the lasing wavelength, a process known as the electronic tuning of semiconductor lasers. The main physical mechanisms that link changes in the current to changes in the refractive index are (i) the free-carrier plasma effect, (ii) the quantum-confined Stark effect (QCSE) as well as (iii) the temperature[11] and (iv) gain dependence of the refractive index. In this work, the temperature was kept constant (iii) and the QCSE (ii) was not included into our simulation model. Refractive index changes due to carrier injection into the semiconductor can be estimated by:[12]

$$\Delta n = -\frac{e^2\lambda^2}{8\pi^2 c^2 n\varepsilon_0}\left(\frac{N}{m_e}+\frac{P}{m_h}\right) = -\frac{6.9\cdot 10^{-22}}{nE^2}\left(\frac{N}{m_e}+\frac{P}{m_h}\right) \tag{1}$$

where λ is the photon wavelength, m_e and m_h are the effective masses of the injected electrons ($0.18\ m_0$) and holes ($0.95\ m_0$),[13] respectively, n is the refractive index of the semiconductor, E is the photon energy in eV, and N and P are the concentration of electrons and holes, respectively, in cm^{-3}. Note that the refractive index decreases with increasing current. As the refractive index reduction is inhomogeneous, we estimated the effective refractive index changes by the formula:[14]

$$\Delta n_{eff} = \frac{\int_{-\infty}^{\infty} E^2(x)\Delta n(x)dx}{\int_{-\infty}^{\infty} E^2(x)dx} \tag{2}$$

where $E(x)$ is the amplitude of the electric field in the vertical direction.

The free-carrier concentration was simulated using the commercial software SiLENSe (Fig. 2(a)). McConville *et al.*[15] and Asryan *et al.*[16] suggest that non-pinning of the free-carrier concentration above the threshold current might occur due to violations of charge neutrality in the active region. Therefore we have made calculations for both cases, including pinning and non-pinning of the free-carrier concentration. For an increase in current from 540 to 720 mA, the effective refractive index change Δn_{eff} of $-1.9\cdot 10^{-4}$ for the pinning case and $-3.6\cdot 10^{-4}$ for the non-pinning case (Fig. 2(b)) was estimated using Eqs. (1) and (2). These simulations show that, even in the pinning case, Δn_{eff} will change due to an increased free-carrier concentration outside the active region, mainly in the electron blocking and waveguide layer (Fig. 2(b)). The gain in the active layers of the laser structure can be represented by an imaginary part of the refractive index. The change in the real part of the refractive index due to the change in the imaginary part is connected by the Kramers–Kronig relationship:[17]

$$\Delta n(E) = -\frac{\hbar c}{\pi} P\int_0^{\infty} \frac{\Delta g(E') - \Delta g(E)}{E'^2 - E^2} dE' \tag{3}$$

As can be seen in Fig. 3 the refractive index change due to gain does not exceed $+4\cdot 10^{-3}$ for the current increase from 540 to 720 mA. Taking into account that refractive index change occurs only in the active layers with optical confinement factor Γ of 2.1%, the effective refractive index change is estimated by $\Delta n_{\text{eff}} = \Gamma\cdot\Delta n = +0.8\cdot 10^{-4}$. In combination with the free-carrier effect, this results in the total calculated effective refractive index change of $-1.1\cdot 10^{-4}$ for the free-carrier pinning case and $-2.8\cdot 10^{-4}$ for the non-pinning case.

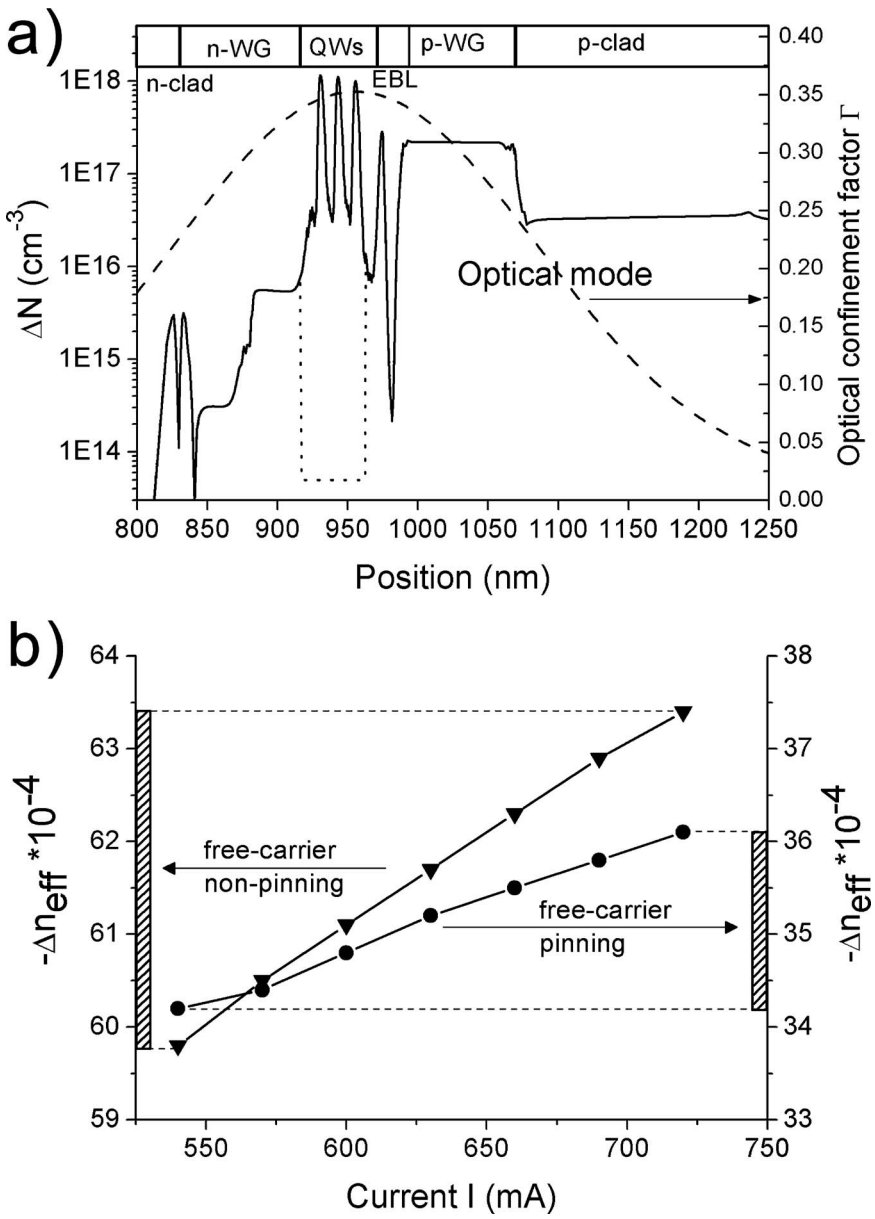

FIG. 2. (a) Simulation of the difference in electron density ΔN between 540 and 720 mA injection currents (current density 9.9 and 13.1 kA/cm^2, respectively). Free-carrier pinning above the threshold is indicated by the dotted line. (b) Effective refractive index change with free-carrier pinning (circles) and non-pinning (triangles) as a function of injected current.

The change of the effective refractive index of the laser will translate into a change in the operation wavelength, which for a single-cavity Fabry–Perot laser is defined by:[18]

$$\Delta\lambda = \lambda_0 \frac{\Delta n_{eff}}{n_{g,eff}} \tag{4}$$

where λ_0 is the center lasing wavelength, Δn_{eff} is the change in the effective refractive index and $n_{\text{g,eff}} = 3.388$ is the group effective refractive index. However, the continuous tuning range is limited by the possible effective index change. For the refractive index changes mentioned above, a tuning range of only 0.03 nm is available according to Eq. (4). However, by using the Vernier tuning mechanism in the coupled cavity laser, the tuning range can be increased significantly compared to a conventional single-cavity laser.[19] With Vernier tuning the lasing mode jumps from one longitudinal

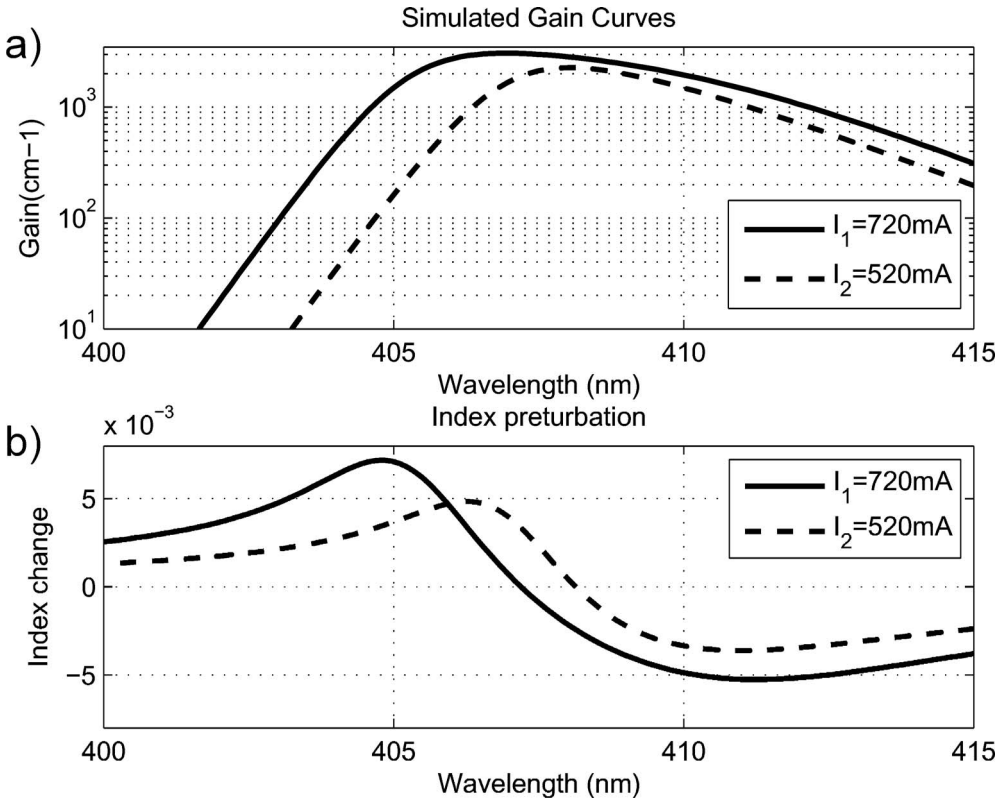

FIG. 3. (a) Simulated gain curves and (b) calculation of the refractive index change due to the gain difference for minimum (540 mA) and maximum (720 mA) currents used during tuning measurements.

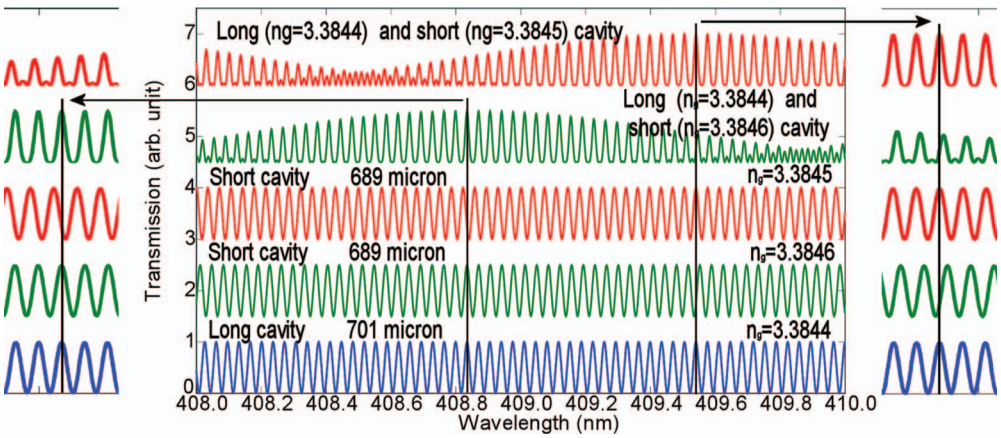

FIG. 4. Fabry-Perot resonances calculated when the refractive index of the long cavity is kept constant (blue) and the short cavity ones is varied (green and red). The resonances calculated for the coupled system show mode switching due to Vernier effect. All curves are shifted vertically for clarity.

mode to another. It is worth mentioning that, if the refractive index decreases in the short cavity, the lasing mode shifts to a longer wavelength (see Fig. 4). At the same time, if the refractive index decreases in the long cavity, the lasing mode shifts in the opposite direction to a shorter wavelength.

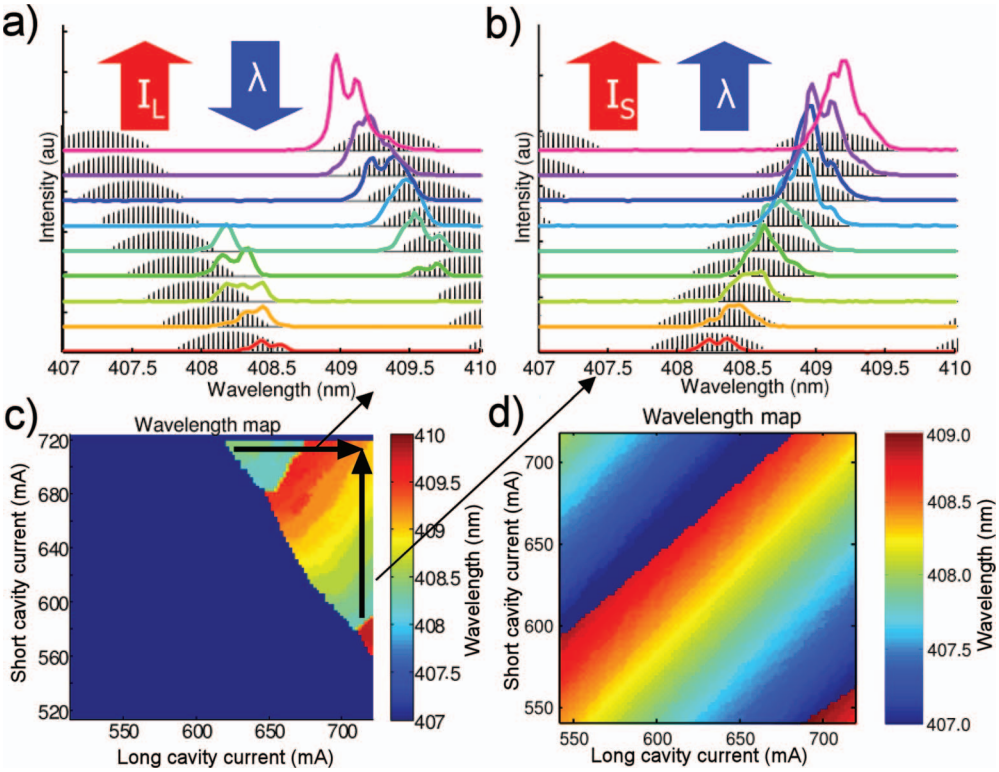

FIG. 5. Experimental lasing spectra (color) as a function of increasing current in the (5 a) long and (5 b) short cavity. The Fabry-Perot resonances, that experience low optical losses (shown in black) were simulated: n_g.=3.388 and refractive index decrease due to carrier injection according to free carrier pinning case (Fig. 2(b)) being from – (35.0 to 36.0) $\cdot 10^{-4}$ for the long cavity scan(a) and from – (34.5 to 36.0) 10^{-4} for the short cavity scan (b). All spectra shifted vertically for clarity. (c) Experimental and (d) simulated wavelength map. Color represents the lasing wavelength as a function of current in the long cavity (horizontal axis) and short cavity (vertical axis).

V. EXPERIMENTAL RESULTS

The spectral tuning characteristics of the laser are shown in Fig. 5. The experimental wavelength map in Fig. 5(c) shows the lasing wavelength as a function of the short and long cavity currents. The sections of this map (see Figs. 5(a) and 5(b)) visualize the spectral behavior when one of the currents is kept constant while another is increased. The experimental wavelength map is in good qualitative agreement with predictions obtained with the Vernier theory.

An increase in current decreases the refractive index as a result of the free-carrier plasma effect. A decrease in the refractive index in the long cavity causes a blue shift (Fig. 5(a)), whereas the same decrease in the short cavity causes a red shift (Fig. 5(b)) of the laser emission. Both effects combined result in a diagonally striped wavelength map (Fig. 5(c)). The main mechanism of the tuning is Vernier effect, meaning Fabry-Perot resonances coincidence in the short and long cavities. Multiple neighboring resonances can lase at the same time taking into account mode spacing of 35 pm. Small refractive index variations in one of the cavity shifts its Fabry-Perot resonances and makes other Fabry-Perot resonances to coincide, thus providing tuning.[18] If resonances in one of the cavities is shifted more than spacing between the resonances in another cavity the jump in tuning will happen (Fig. 5(a)) and cycle repeat itself slightly shifting in wavelength. The laser threshold was found to be around 650 mA per cavity, which corresponds to a current density of 11.9 kA/cm^2. This value is relatively high compared to that of state-of-the-art InGaN/GaN lasers.[20] We believe this can be improved by further optimizing the laser diode efficiency as well as the sidewall roughness and angle of the air slot fabricated by FIB. Laser emission is multimode, which is expected for 7.8-μm-wide laser ridges with an average full width at half maximum (FWHM) of 0.3 nm.

A model based on steady-state solutions of rate equations[21] has been used to simulate the wavelength map. The simulated wavelength map is shifted by about 1.0 nm to the shorter wavelength compared to the experimental one. In our simulation model gain curves calculated with the commercial software SiLENSe were used. The simulated gain curves might have gain maximum at slightly different wavelength due to fabrication uncertainties of the quantum well thickness. The best fit between the calculated and experimental wavelength maps (Figs. 5(c) and 5(d)) occurs at a total refractive index change of $-1.5 \cdot 10^{-4}$, which is closer to $-1.1 \cdot 10^{-4}$ than to $-2.8 \cdot 10^{-4}$ for free-carrier pinning and non-pinning, respectively. This result suggests that the measured device deviates from an ideal laser model and that free-carrier non-pinning partly occurs.[15,16] The experimental tuning range of 1.6 nm is slightly smaller than the simulated value[21] of 1.9 nm (Fig. 5(d)).

VI. CONCLUSIONS

In summary, we have demonstrated electronic tuning of an integrated coupled-cavity GaN/InGaN multiple quantum well laser at 409 nm. The measured electronic tuning range is 1.6 nm. Multimode emission was observed with an average spectral FWHM of 0.3 nm. The experimental data indicates an effective refractive index change of $-2.5 \cdot 10^{-4}$ for the currents used. Our simulations show the significant effective refractive index change even for the free-carrier pinning case due to the increase in the free-carrier concentration outside the active layers. Free-carrier injection is the predominant mechanism of the refractive-index change for the laser under the operational conditions described in this work.

ACKNOWLEDGMENTS

The authors acknowledge Hozanna Miro and Paul Alkemade for valuable discussions on FIB fabrication optimization. This work was funded by the SenterNovem (Agentschap NL) within the scope of the Dynamic Blue project (IS071025) and the National Center for Research and Development in Poland.

[1] M. A. Dubinski and P. Misra, *Ultraviolet Spectroscopy and UV Lasers* 1st ed. (CRC, New York, 2002).
[2] C. Zimmermann, V. Vuletic, A. Hemmerich, and T. W. Hansch, Appl. Phys. Lett. **66**, 2318 (1995).
[3] D. J. Armstrong and A. V. Smith, IEEE J. Sel. Top. Quantum Electron. **13**, 721 (2007).
[4] E. D. Stokes, F. B. Dunning, R. F. Stebbings, G. K. Walters, and R. D. Rundel, Opt. Commun. **5**, 267 (1972).
[5] D. Jaque, J. Capmany, and J. García Solé, Appl. Phys. Lett. **75**, 325 (1999).
[6] J. Hult, Iain S. Burns, and Clemens F. Kaminski, Appl. Opt. **44**, 3675–3685 (2005).
[7] K. Komorowska, P. Wisniewski, R. Czernecki, P. Prystawko, M. Leszczynski, T. Suski, I. Grzegory, S. Porowski, S. Grzanka, M. Maszkowicz, and P. Perlin, Proc. SPIE **6485**, 648502 (2007).
[8] S. Forget, H. Rabbani-Haghighi, N. Diffalah, A. Siove, and S. Chénais, Appl. Phys. Lett. **98**, 131102 (2011).
[9] W. T. Tsang, N. A. Olsson, and R. A. Logan, Appl. Phys. Lett. **42**, 650 (1983).
[10] I. Grzegory, J. Phys.: Condens. Metter **14**, 11055 (2002).
[11] J. Buus, M.-C. Amann, and D. J. Blumenthal, *Tunable laser diodes and related optical sources* 2nd ed. (John Wiley & Sons, 2005), p. 96.
[12] C. H. Henry, R. A. Logan, and K. A. Bertness, J. Appl. Phys. **52**, 4457 (1981).
[13] M. Suzuki, T. Uenoyama, and A. Yanase, Phys. Rev. B **52**, 8132 (1995).
[14] Takahiro Numai, *Fundamentals of Semiconductor Lasers* (Springer, 2004), p. 50.
[15] D. G. McConville, S. J. Sweeney, A. R. Adams, S. Tomic, and H. Riechert, Phys. Stat. Sol. (b) **244**, 208 (2007).
[16] L. V. Asryan, S. Luryi, and R. A. Suris, IEEE J. Quantum Electron. **39**, 404 (2003).
[17] G. Hunziker, W. Knop, P. Ungen, and C. Harder, IEEE J. Quantum Electron. **31**, 643 (1995).
[18] J. Buus, M.-C. Amann, and D. J. Blumenthal, *Tunable laser diodes and related optical sources* 2nd ed. (John Wiley & Sons, 2005), p. 89.
[19] S. Höfling, J. Heinrich, J. P. Reithmaier, A. Forchel and J. Seufert, Appl. Phys. Lett. **89**, 241126 (2006).
[20] R. M. Farrell, P. S. Hsu, D. A. Haeger, K. Fujito, S. P. DenBaars, J. S. Speck, and S. Nakamura, Appl. Phys. Lett. **96**, 231113 (2010).
[21] D. Marcuse and N.-P. Lee, IEEE J. Quantum Electron. **20**, 166 (1984)